Comprehensive deep learning for combustion chemistry integration: Multi-fuel generalization and *a posteriori* validation in reacting flow ⊘

Han Li (李晗) (iD); Ruixin Yang (杨瑞鑫); Yangchen Xu (徐阳晨); Min Zhang (张敏); Runze Mao (毛润泽);
Zhi X. Chen (陈帜) ✉ (iD)

Check for updates

View Online   Export Citation

Articles You May Be Interested In

Graphics processing unit/artificial neural network-accelerated large-eddy simulation of swirling premixed flames

Physics of Fluids (May 2024)

A posteriori analysis of numerical errors in subfilter scalar variance modeling for large eddy simulation

Physics of Fluids (March 2011)

A priori and *a posteriori* analysis of flamelet modeling for large-eddy simulations of a non-adiabatic backward-facing step

Physics of Fluids (May 2023)

Comprehensive deep learning for combustion chemistry integration: Multi-fuel generalization and *a posteriori* validation in reacting flow

View Online   Export Citation   CrossMark

Han Li (李晗),[1,2] (iD) Ruixin Yang (杨瑞鑫),[1,2] Yangchen Xu (徐阳晨),[1] Min Zhang (张敏),[3] Runze Mao (毛润泽),[1,2]
and Zhi X. Chen (陈帜)[1,2,a] (iD)

AFFILIATIONS

[1]State Key Laboratory of Turbulence and Complex Systems, College of Engineering, Peking University, Beijing 100871, China
[2]AI for Science Institute (AISI), Beijing 100080, China
[3]School of Energy Science and Engineering, Central South University, Changsha 410083, China

Note: This paper is part of the Special Topic, ISPF9 (9th International Symposium on Physics of Fluids).
[a]Author to whom correspondence should be addressed: chenzhi@pku.edu.cn

ABSTRACT

The application of deep neural networks (DNNs) holds considerable promise as a substitute for the direct integration of combustion chemistry in reacting flow simulations. However, challenges persist in ensuring high precision and generalization across various fuels and flow conditions, particularly in *a posteriori* time-evolving flame simulations. This study performs comprehensive deep learning with multi-fuel generalization and computational fluid dynamics (CFD) validations. The process begins with generating thermochemical base states from low-dimensional canonical laminar flames to facilitate generalization and minimize the complexity of data generation. An effective perturbation and data augmentation strategy is then employed to broaden the coverage of the composition space for multi-dimensional flame configurations. Without the need for extensive tuning, three DNNs were consistently trained for three representative fuels: hydrogen, ethylene, and Jet-A. These DNN models were subsequently integrated into our recently developed open-source CFD package, DeepFlame (https://github.com/deepmodeling/deepflame-dev), for *a posteriori* reacting flow simulations and thoroughly validated against laminar flames and two representative turbulent premixed flames. The DNNs strongly agreed with the direct integration results across various combustion characteristics, including laminar and turbulent flame speeds, dynamic flame structures influenced by turbulence-chemistry interactions, and conditional scalar profiles. These findings underscore the exceptional accuracy and generalization capability of the employed deep learning approach. Moreover, by leveraging graphics processing units for model inference, the integration of DNN into CFD simulations resulted in significant speed-ups, achieving factors of approximately 72 for ethylene/air flames and 102 for Jet-A/air flames. The integrated DNN-CFD solver and test cases (https://www.aissquare.com) are openly shared, providing valuable tools to advance DNN development for chemical kinetics.

I. INTRODUCTION

The utilization of finite rate chemistry (FRC) in combustion modeling typically yields a more comprehensive and accurate depiction of reaction processes and flame dynamics, when compared to the simplified representations offered by global reactions or flamelet-generated manifolds (FGM). However, detailed FRC modeling entails a substantial computational cost driven by direct integration (DI) of stiff ordinary differential equations (ODEs).[1] To enhance computational efficiency, various methods for simplifying ODEs, including chemical mechanism reduction,[2–7] have been developed. These

methods focus on eliminating non-essential species and reactions from detailed mechanisms to minimize the number of ODEs. However, even with a reduced mechanism that typically retains several tens of chemical species exhibiting markedly distinct chemical time scales, DI of the associated ODEs remains an expensive task, constituting over 80% of the total computational cost in practical combustion simulations. This computational burden significantly hinders the widespread application of the FRC approaches.

To tackle the challenge of balancing accuracy and efficiency, recent strides in artificial intelligence (AI) for scientific applications,

09 January 2025 09:22:57

notably in machine learning (ML), have opened up innovative perspectives.[8] In the present work, we focus on employing ML models to replace DI with a similar level of accuracy. As a pioneering work, Christo et al.[9] developed a neural network (NN) to represent a three-step mechanism in the joint probability density function (PDF) simulation of turbulent jet flames, showcasing the substantial potential of ML in combustion modeling. Blasco et al.[10,11] proposed a self-organizing map (SOM) approach with an enhanced precision in predicting the temporal evolution of reactive species. However, the aforementioned works relied on training the NN on the specific problem of interest with limited range of applicability. To address this issue, Sen and Menon[12,13] obtained thermochemical states from direct numerical simulation (DNS) and linear eddy mixing (LEM) model calculations, and proved successful in simulating syngas/air flames. Chatzopoulos and Rigopoulos[14] collected samples from non-premixed laminar flames and using the SOM technique to train NN models. These models were subsequently applied to Reynolds Averaged Navier–Stokes (RANS)-PDF simulations of DLR jet flames. In a follow-up work, Franke et al.[15] integrated extinguishing flamelets into the training dataset. Recently, Wan et al.[16] generated training samples from a non-premixed micro-mixing canonical problem and then achieved good agreement with the DI approach in a syngas turbulent oxy-flame. Ding et al.[17] and Readshaw et al.[18] collected samples from numerous 1D laminar flames and randomized these data for training using multiple NNs (three for each species). The resulting NNs were tested to be effective on methane/air flames, including one-dimensional laminar flame and Sandia turbulent jet flames. In contrast to sampling from low-dimensional flames, Zhang et al.[19] introduced a multi-scale sampling method to collect data from the full composition space. Owing to the powerful fitting capability of deep neural network (DNN), they trained a rather *big model* using a large dataset comprising over 5×10^6 samples, covering a broad composition space for hydrogen/air flames. With over 1.6×10^6 model parameters, this DNN showed a good generalization capability across a range of laminar and turbulent flames under various conditions.

The usefulness of ML models essentially relies on achieving both high accuracy and generalization ability. Previous studies employing a multiple layer perceptron (MLP) architecture such as the SOM-MLP approach[10,14] and multiple MLP (MMLP)[18] have demonstrated improved accuracy. Effective generalization has also been achieved by collecting training data from simple canonical problems.[14–18] However, the validation of these ML models was predominantly limited to canonical problems and a specific multi-dimensional turbulent flame, leaving the generalization for other turbulent flame configurations unexplored. Furthermore, prior research has primarily focused on a single and simple chemical system with a small number of chemical species, such as hydrogen, methane, and syngas. Limited attention has been given to the generalization ability across different and complex fuels, like large hydrocarbons, whose reduced mechanisms comprise dozens of chemical species.

With this motivation, the primary objective of the present work is to explore a consistent and robust deep-learning framework for generating generic samples, training high-precision DNNs, and comprehensively assessing their validity across a spectrum of fuels ranging from simple hydrogen to complex kerosene and in different turbulent premixed flame configurations. Specifically, three DNNs are trained for reactive mixtures of hydrogen/air with a 9-species mechanism,[20]

ethylene/air with a 24-species mechanism,[21] and Jet-A/air with a 41-species mechanism,[22] respectively. The model deployment and *a posteriori* assessment are then performed using our recently developed open-source code DeepFlame,[23,24] which interfaces OpenFOAM, Cantera, and PyTorch libraries. Two typical turbulent premixed flame cases are considered: a temporally evolving jet flame and a propagating flame kernel in homogeneous isotropic turbulence (HIT). The DNN models, computational fluid dynamics (CFD) codes, and test cases presented in this study are made available for community data sharing and reproducibility.

The remainder of this paper is organized as follows: In Sec. II, a brief problem statement is provided regarding chemistry integration in combustion simulations. Section III discusses the methodology for generic DNN training. In Sec. IV, we present the turbulent CFD case setups for model validation. In Sec. V, the results for different fuels and chemical mechanisms are discussed. Conclusions are summarized in Sec. VI.

II. MODELING PROBLEM

In combustion modeling, chemical reaction kinetics are essential for predicting the rates of formation and consumption of each species. The reaction rates are typically governed by the Arrhenius equation,

$$k = A \exp\left(\frac{-E_a}{RT}\right), \tag{1}$$

where k is the reaction rate constant, A is the pre-exponential factor, E_a is the activation energy, R is the universal gas constant, and T is the temperature. This equation highlights the temperature dependence of reaction rates, which directly influences the rate at which chemical species react. For a chemical system involving multiple species, the reaction rates define the time evolution of species concentrations through a set of coupled ordinary differential equations (ODEs),

$$\frac{d(\rho Y_i)}{dt} = W_i \dot{\omega}_i = W_i \sum_{j=1}^{N_r} (\nu_{ij}'' - \nu_{ij}') q_j, \tag{2}$$

$$q_j = k_{fj} \prod_{k=1}^{N_{sp}} [X_k]^{\nu'_{kj}} - k_{rj} \prod_{k=1}^{N_{sp}} [X_k]^{\nu''_{kj}}, \tag{3}$$

where ρ is the density of the mixture, Y_i, $\dot{\omega}_i$, and W_i are the mass fraction, the net production rate and the molecular weight of species i, respectively. ν_{ij} is the stoichiometric coefficient of species i in reaction j. The superscript $'$ indicates forward stoichiometric coefficients, while $''$ indicates reverse stoichiometric coefficients. q_j is the rate of progress variable of reaction j. k_{fj} and k_{rj} are the forward and reverse reaction rate constant for reaction j, respectively. X_k is the molar concentration of species k, N_r is the number of reactions, and N_{sp} is the number of species in the chemical mechanism.

Solving these stiff ODEs, which involve vastly different chemical time scales, is computationally expensive. To overcome this challenge, deep neural networks (DNNs) are introduced as an efficient alternative. Rather than directly integrating the ODE system at each time step, DNNs are trained to approximate the reaction rates and thermochemical states, significantly reducing computational cost. The neural network, denoted as $\mathscr{F}_\theta$, can approximate the solution,

$$\left(Y_1, ..., Y_{N_{sp}}\right)_{t+\Delta t} = \mathscr{F}_\theta(T, P, Y_1, ..., Y_{N_{sp}})_t, \tag{4}$$

where $\mathscr{F}_\theta$ is the trained neural network with parameters θ, predicting the future thermochemical state based on the current state, bypassing the need for direct ODE integration.

III. DEEP LEARNING METHODOLOGY

This section describes the step-by-step procedures for the deep learning approach designed to replace the direct integration of combustion chemistry. It covers training data generation and sampling, network design and hyperparameter tuning, and model prediction testing. These procedures are consistently applied across a range of fuels and premixed turbulent flame configurations considered in this study.

A. Thermochemical base state generation

Due to the highly non-linear and stiff nature of chemical ODE systems, the error tolerance allowed for reaction rate integrator is extremely stringent. Thus, it is imperative to generate representative training data that encompass a proper distribution of thermochemical states and thoroughly covers the relevant composition space.

Instead of directly exploring the high-dimensional thermochemical sampling space, we first locate a low-dimensional manifold region as the base state. This does not necessarily imply a flamelet assumption but provides a good starting point for the sampling process. In this study, the thermochemical base states are collected from simulations of a set of canonical laminar premixed flames to ensure generalization and also to minimize the complexity of data generation. This approach can be easily extended to diffusion flames and other canonical configurations. The computational domain of these 1D laminar flames is initialized with premixed fuel/air mixture in one half and equilibrium states are set in the other half. The initial conditions (i.e., temperature, pressure, and equivalence ratio) are set according to the global parameters of the target turbulent flames. Simulations are conducted until steady states are reached. The simulated time of each 1D flame is estimated to be around ten times the respective chemical timescale $\tau_{chem} = \delta_L/S_L$, and the temporal thermochemical states are sampled every 100 simulation time steps.

B. Data perturbation and augmentation

The thermochemical states obtained from laminar flames might not comprehensively cover the relevant composition space in *a posteriori* applications. More critically, these particular states follow an exact path in the sample space (essentially flamelet manifolds), and hence, the trained model is susceptible to perturbations, i.e., deviation from the manifold in the thermochemical state. To address this issue and enhance model robustness, a data augmentation strategy is applied to perturb the collected states, mimicking the multi-dimensional transport and turbulence perturbations. At each sample point, temperature, pressure, and inert species are randomly perturbed using[18]

$$x_R = x + \alpha * \beta * (x_{max} - x_{min}), \tag{5}$$

where x_R and x represent the temperature, pressure, or inert species mass fraction of the perturbed samples and the original samples, respectively. The perturbation amplitude α is user-specified and β is a uniformly randomized number within the range $(-1,1)$. The perturbation amplitude α and number of randomization times N_R can be adjusted according to the amount of collected states and the turbulence

intensity of the flow field. In this work, we use $\alpha \in [0.1, 0.15]$ and $N_R = 10$ perturbations for all three fuels considered. Given the significant changes in mass fraction magnitudes for reactive chemical species, a different exponential randomization strategy is implemented,

$$y_R = y^{1+\alpha*\beta}, \tag{6}$$

where y_R and y represent the species mass fraction (excluding inert species) of the perturbed samples and the original samples, respectively. The resulting randomly generated mass fractions of these species Y_R^i are normalized to $1 - x_R^{N_2}$ as follows:

$$Y_R^i = y_R^i \frac{1 - x_R^{N_2}}{\sum y_R^i}, \tag{7}$$

for mass conservation consideration. A comparison was conducted to evaluate the effectiveness of the proposed randomization and normalization strategy (denoted as approach *A*) by contrasting it with two alternative approaches: perturbing all species mass fractions using x_R and normalizing them to unity (denoted as approach *B*); perturbing all species mass fractions using x_R and normalizing them excluding inert gas to $1 - x_R^{N_2}$ (denoted as approach *C*). The results, shown in Fig. 1, clearly demonstrate the necessity of the proposed randomization and normalization strategy, as it leads to significantly improved prediction accuracy in capturing the flame structure, with particular attention to temperature and species mass fractions.

Following the above strategy, the coverage of the composition space is substantially enhanced. However, it may generate numerous nonphysical states if left unconstrained, which lowers the model accuracy in the regions of interest. To address this, a threshold criterion, based on the heat release rate (HRR) change between the original collected state and the perturbed state, is applied to filter out nonphysical perturbed states for improved accuracy and generalization ability. In this study, perturbed states with HRR values exceeding 100 times above or below the original HRR values are deemed invalid states and subsequently discarded. Through these augmentation and filtering steps, a high-quality training dataset is generated. Taking ethylene/air flames as an example, Fig. 2 illustrates the spatial distributions of the sampled low-dimensional states, augmented and filtered states for training, and samples from *a posteriori* simulations. Specifically, the mass fractions of major species and the heat release rate are plotted against temperatures, indicating changes with reaction progress. In the figure, the manifold-like orange symbols represent states collected from 1D laminar flames, the scattered blue symbols depict the physics-constrained random perturbation states, and the green symbols are sampled from a 2D turbulent flame. It is clear that the 1D flame manifold closely resembles that of the 2D turbulent flame, though it has a more limited composition space. With the proposed data augmentation strategy, the coverage of the composition space is significantly broadened while preserving the key features of the original physical composition. This demonstrates the effectiveness of the augmentation approach in expanding the input space for neural network models, with the random perturbation successfully mimicking the distribution observed in turbulent flames, validating the approach.

C. Deep neural network training

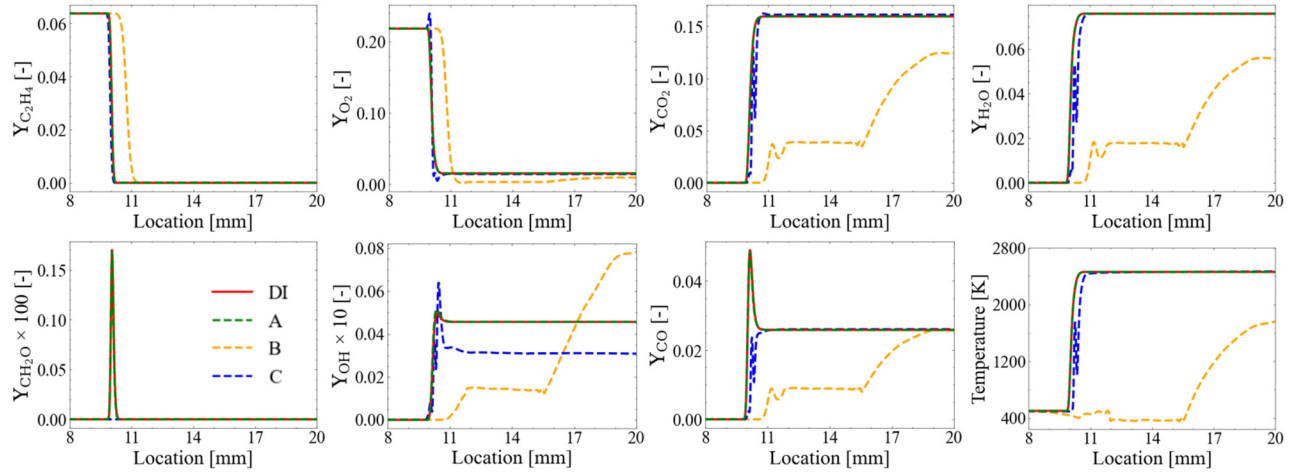The DNN input layer includes temperature, pressure, and species mass fractions, represented as

FIG. 1. Comparison of the performance of different randomization and normalization approaches: *A* (green), *B* (orange), and *C* (blue) on reproducing the laminar flame spatial distribution of temperature and major species mass fraction calculated by direct integration (red).

$$\boldsymbol{x}(t) = \left\{ T(t), P(t), \mathscr{F}_{BCT}[\boldsymbol{Y}(t)] \right\}. \tag{8}$$

The output layer consists of the change of species mass fraction over a given time step size, denoted as

$$\boldsymbol{u}^*[\boldsymbol{x}(t), \Delta t] = \mathscr{F}_{BCT}[\boldsymbol{Y}(t + \Delta t)] - \mathscr{F}_{BCT}[\boldsymbol{Y}(t)], \tag{9}$$

where $\mathscr{F}_{BCT}$ is the Box-Cox transformation (BCT)[25] employed for the multi-scale species mass fractions. This transformation provides a more uniform distribution of small-scale clustered sample data, thereby enhancing the performance of the neural network in predicting the species mass fraction changes.[19] The BCT formula is given by

$$\mathscr{F}_{BCT}(y) = \begin{cases} \dfrac{y^\lambda - 1}{\lambda}, & \lambda \neq 0, \\ \log(y), & \lambda = 0, \end{cases} \tag{10}$$

where y is species mass fraction and λ is a hyper-parameter. The training dataset $D = \{\boldsymbol{x}_i, \boldsymbol{u}_i^*\}_{i=1}^N$, with N samples, undergoes Z-score normalization, where both the input and output undergo mean subtraction and division by standard deviation.

The next step involves applying a MLP as the DNN model for function approximation. The MLP structure comprises an input layer with $N_{sp} + 2$ neurons (corresponding to the number of species along
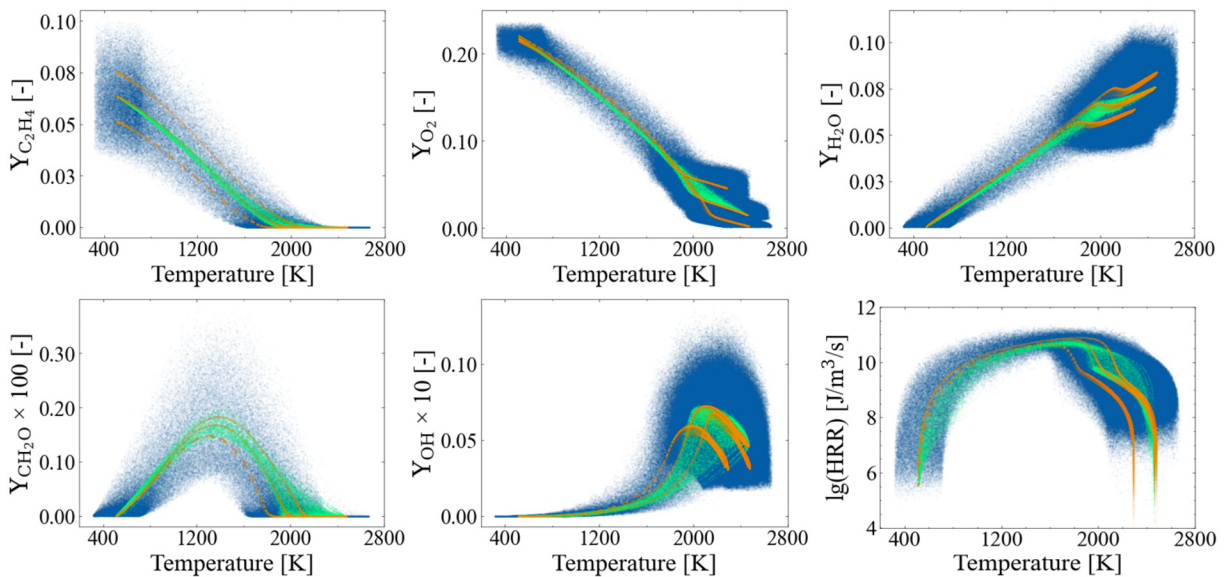

FIG. 2. Joint distribution of major species mass fraction and heat release rate (HRR) as a function of temperature for low-dimensional thermochemical base state (orange), high-dimensional *a posteriori* case (green) and perturbed state (blue) in ethylene/air flames.

with temperature and pressure) and one output layer with $N_{sp} - 1$ neurons. The output corresponds to the changes in species mass fractions, excluding the inert species, which remain constant and thus do not require prediction. Between the input and output layers, four hidden layers are employed, each with the same number of neurons. This architecture strikes a balance between capturing the intricate, nonlinear dependencies of the input features and efficiently approximating the output variables. The MLP uses the Gaussian error linear unit (GELU) as its activation function, which improves the training dynamics by offering smoother activation behavior. Hyper-parameter tuning is carried out using the Adam optimization algorithm employing an 80–20 training-validation split to ensure model generalization. The maximum number of epochs is set to 1500, with an initial learning rate of 1×10^{-3}, which decays to 1×10^{-5} as training progresses. It is essential to note that the DNN predictions yield only the change of species mass fractions. The temperature and density are subsequently computed based on enthalpy and mass conservation laws, ensuring physically consistent results. A common loss function of mean absolute error (MAE, $L1$ loss) for constraining the DNN output is utilized and expressed as follows:

$$L = \frac{1}{N} \sum_{i=1}^{N} |\boldsymbol{u}_i - \boldsymbol{u}_i^*|, \tag{11}$$

where $\boldsymbol{u}_i$ is the DNN output. The training $||L1||$ loss on $\mathscr{F}_{BCT}[\boldsymbol{Y}(t)]$ is observed to be on the order of 10^{-3}. Figure 3 illustrates the trend of loss values as a function of training epochs for the ethylene/air DNN model. As shown, the training loss exhibits a gradual decline, initially with slight fluctuations, but stabilizes over time. Importantly, it aligns closely with the validation loss, indicating a well-generalized model that effectively captures the underlying data patterns without overfitting.

Once the DNN model is trained, *a priori* test is performed to evaluate the prediction errors in a straightforward manner. This step is crucial before subsequent validation using reacting flow cases. As an example, here we consider the DNN model for ethylene/air mixture and the results are similar for other fuels. Figure 4 shows the predictions for the fuel species C_2H_4, oxidizer O_2, important radicals, and product species. It can be seen that the predicted values are in excellent agreement with the randomly chosen label values. The root mean square errors (RMSE) are of the order of $10^{-8} \sim 10^{-6}$, which is expected to satisfy the chemical ODE requirement in various laminar and turbulent flames.
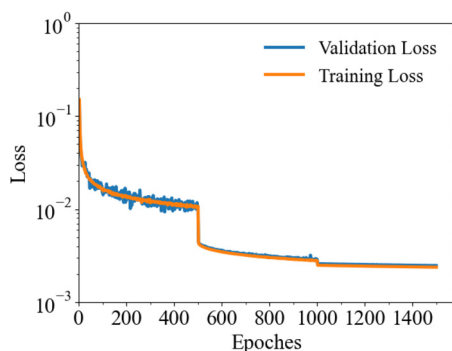

FIG. 3. Training loss and validation loss for ethylene/air DNN model.

D. Fully integrated CFD package with AI and graphics processing unit (GPU)

The trained DNN models are integrated into our recently developed open-source CFD package, DeepFlame,[23,24] functioning as deep learning-based chemical ODE integrators that replace conventional numerical integrators like CVODE. DeepFlame is a deep learning-empowered CFD package designed for simulating laminar or turbulent reacting flows across all speed regimes. It integrates the strengths of OpenFOAM, Cantera, and PyTorch, enabling deep learning-assisted reacting flow simulations with the potential to leverage next-generation heterogeneous supercomputing and AI acceleration infrastructures, including Graphics Processing Units (GPUs). The workflow after DNN model integration is illustrated schematically in Fig. 5. Specifically, after solving the continuity and momentum equations, the thermochemical states at each grid point are input into the DNN model, which then provides the species production rates to the solver. Following this, the solver advances the species and energy equations. Detailed integration steps can be found in our GitHub repository, with specific references to the pytorchFunctions.H and torchFunctions.H files located in the /src/dfChemistryModel/ folder of the DeepFlame package.

IV. TEST CASE SETUP

To validate the trained DNN models in combustion simulations, two 2D premixed turbulence flame cases are designed and described in this section.

A. Temporally evolving turbulent jet flame

Turbulent planar jets are prototypical free shear flows, which are widely used to study turbulence-chemistry interaction.[26] Here, we present a two-dimensional temporally evolving planar turbulent jet flame, considering the mixing and reaction processes of scalars in turbulent shear flows. A similar configuration has also been utilized by Satio *et al.*[27] to validate their DNN model for ammonia combustion.

As shown in Fig. 6, a square computational domain of $L = 16$ mm is considered, initially filled with stoichiometric fuel/air mixture in the central region and an equilibrium state gas elsewhere. To initialize turbulent shear flow, the internal velocity field is generated from a precursor non-reactive jet flow simulation using the synthetic eddy turbulence inflow generator and then superimposed onto the unburnt gas region. Periodic boundary conditions are applied on the left and right sides, while outlet conditions are set for the top and bottom boundaries. The domain is discretized with 800×550 grids, with a minimum grid size of $20 \, \mu m$ to ensure proper resolution on the flame front. The grid is uniform in the x-direction and stretched at both ends in the y-direction.

B. Ignition in homogeneous isotropic turbulence

The second test case involves a flame kernel ignition of premixed mixture in two-dimensional homogeneous isotropic turbulence (HIT). This simulation setup features an ignition to propagation transition process, highlighting the turbulence effect on the flame evolution.[28] Therefore, it serves as a challenging validation case for the DNN models.

In the simulation, a square computational domain of $L \times L = 10\pi \times 10\pi$ mm^2 is used, initialized with premixed stoichiometric
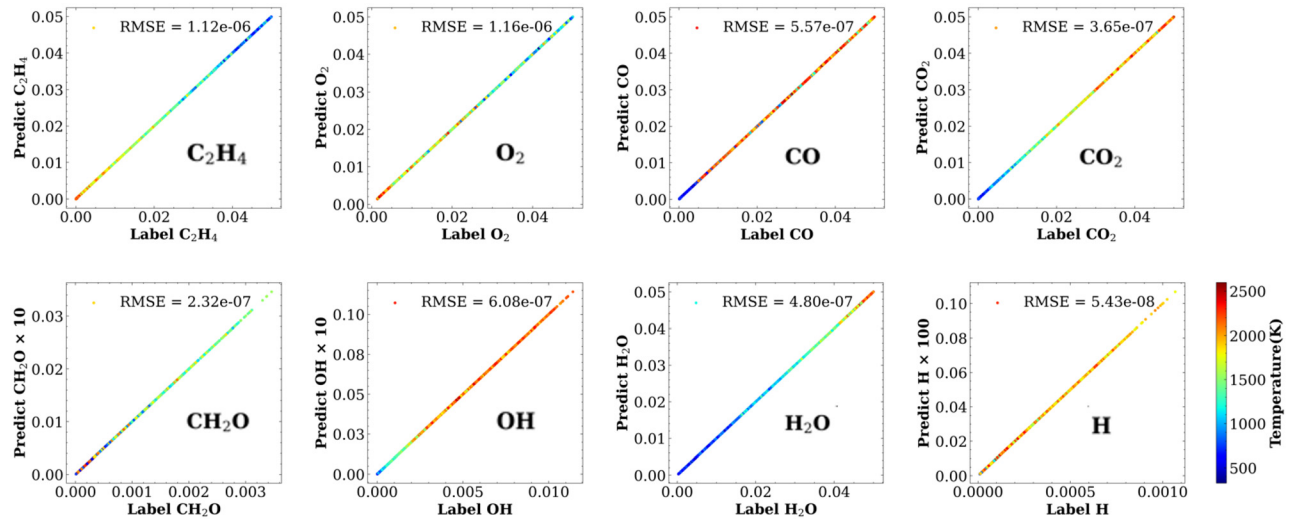
FIG. 4. DNN prediction for typical major and minor species mass fractions colored by the temperature of the sample.

fuel/air mixture at a given temperature and pressure. To ignite the mixture, a circular hot spot with a radius of $L/10$ filled with equilibrium gases is placed in the center of the domain. The HIT generation approach in Ref. 29 is adopted and the fully evolved velocity field is then mapped to the computational domain as the initial flow field. Boundary conditions are set to zero gradient for temperature and

species mass fractions, and a non-reflective wave transmissive condition is used for pressure and velocity. The domain is uniformly discretized with 1024×1024 grids to ensure good resolution for both the flame and turbulence. The simulations are continued until the full domain is ignited.

V. RESULTS AND DISCUSSION

This section presents extensive validations of the proposed methodology and DNN models in various 1D laminar flames and 2D turbulent flames coupling the effects of convection, stretching, and turbulence. All cases are scale-resolved using detailed numerical simulation with detailed chemistry and mixture-averaged transport.[23] The predictions using DNN models are validated against the results obtained through DI using the Cantera CVODE solver. For
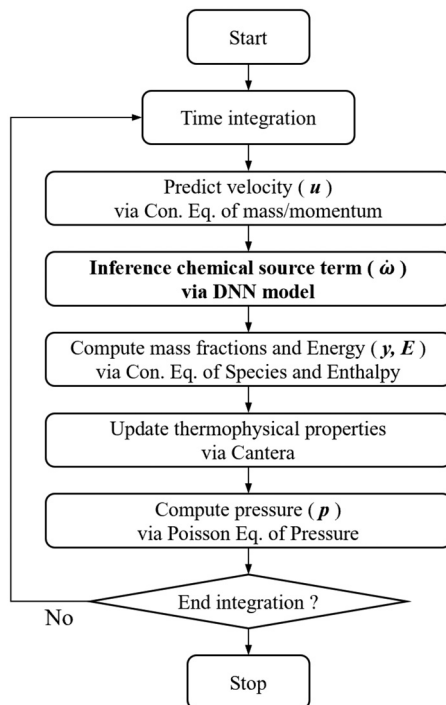

FIG. 5. Schematic flow chart of DeepFlame with integrated DNN model for chemistry integration, taking low-Mach solver as an example.
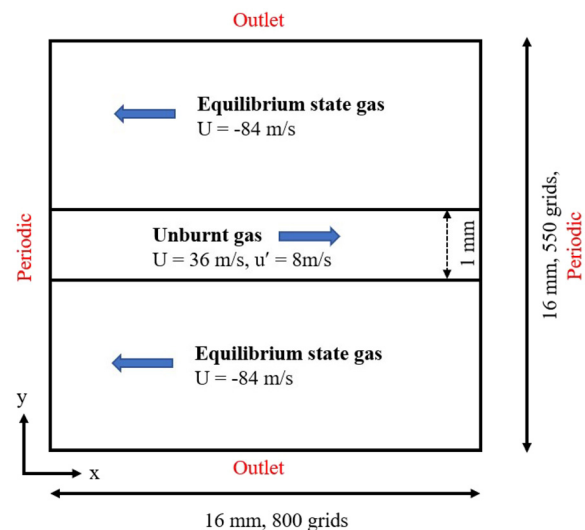

FIG. 6. Computational domain of the 2D evolving jet flame.
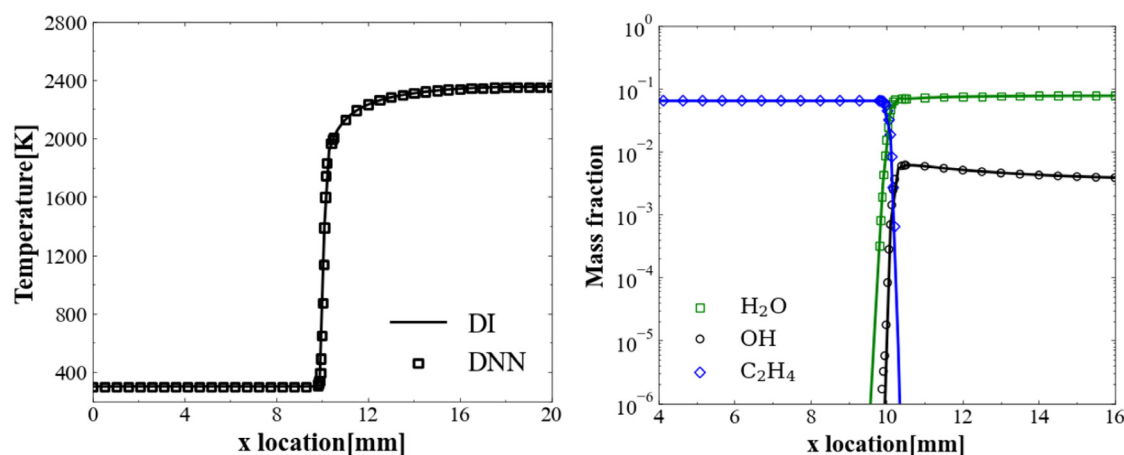
FIG. 7. Spatial distribution of temperature (left) and major species (right) at P = 1 atm, ϕ = 1.0 and T_u = 300 K for ethylene/air.

conciseness, only the ethylene/air combustion results are presented in the main text, with additional results for hydrogen/air and Jet-A/air combustion provided in the supplementary material.

For ethylene/air combustion, thermochemical states are collected from three laminar flame cases with an unburnt gas temperature T_u of 500 K and pressure of 1 atm. The equivalence ratios for the three cases are 0.8, 1.0, and 1.2, respectively. Subsequently, approximately 200 000 state points are collected, perturbed, and augmented to generate a training set of 1 200 000 samples. A time step size of 10^{-7} s is used for DNN model prediction. The training process typically evolves for 1200 epochs, starting with an initial learning rate of 0.001, which is reduced by a factor of 10 at epochs 400, 800, and 1000. Next, the resulting DNN models are tested comprehensively in 1D laminar flames and 2D turbulent flames.

A. 1D premixed laminar flame

Simulations were first conducted on 1D premixed laminar ethylene/air flames over a variety of initial temperatures T_u and equivalence ratios ϕ, to thoroughly evaluate the DNN model's predictive capability across diverse combustion conditions. Figure 7 illustrates the spatial distributions of temperature and major species mass fraction at T_u = 300 K and ϕ = 1.0, with particular focus on the flame front region. The DNN model precisely captures the flame front position and flame structure, with temperature and species profiles that closely align with the DI results. Figure 8 presents calculated laminar flame speeds across equivalence ratios from 0.8 to 1.2. Notably, the test conditions include an initial temperature of T_u = 300 K and equivalence ratios of 0.9 and 1.1, which extend beyond the original data range sampled from low-dimensional manifolds. The DNN predictions closely match the DI results obtained using CVODE, with a maximum predictive error of 1.49%, underscoring the model's ability to accurately capture key flame properties across a wide range of operating conditions. This capability is crucial for robust combustion modeling in practical applications. These tests also confirm that the employed data perturbation and augmentation strategy effectively enhance extrapolation capabilities beyond the thermochemical space of the sampled data, thereby enhancing model generalization.

B. 2D evolving jet flame

Figure 9 illustrates the instantaneous, time-evolving contours of heat release rate in a stoichiometric ethylene/air jet flame, highlighting the detailed flame dynamics and evolution over time. A subset of the domain is presented to provide clarity around the flame front, where complex interactions between combustion and turbulence are prominent. Isolines of CH_2O, with a mass fraction threshold of 5×10^{-4}, are also displayed, capturing the fine-scale radial structure and aiding in the assessment of intermediate species distribution near the flame front. The DNN model results demonstrate excellent agreement with the DI results across all time instants, with no obvious deviation in heat release structure and flame front evolution.

For quantitative assessment, conditional heat release rates and species mass fractions are shown in the progress variable space in Fig. 10. The progress variable is defined as the combined mass fraction of H_2O and CO_2, normalized by their burnt values, providing a metric to track reaction progress. The conditional profiles of heat release and
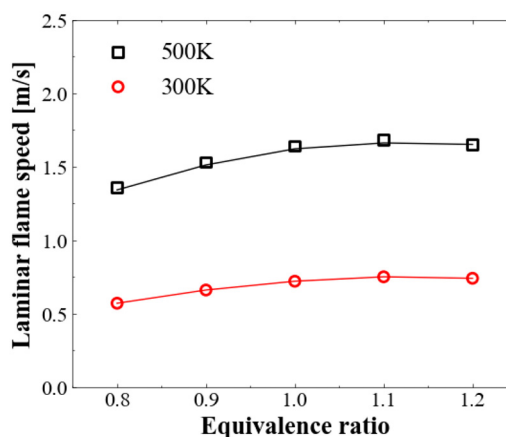

FIG. 8. Laminar flame speed at different equivalence ratios for ethylene/air mixture, predicted using DI (lines) and DNN (symbols).
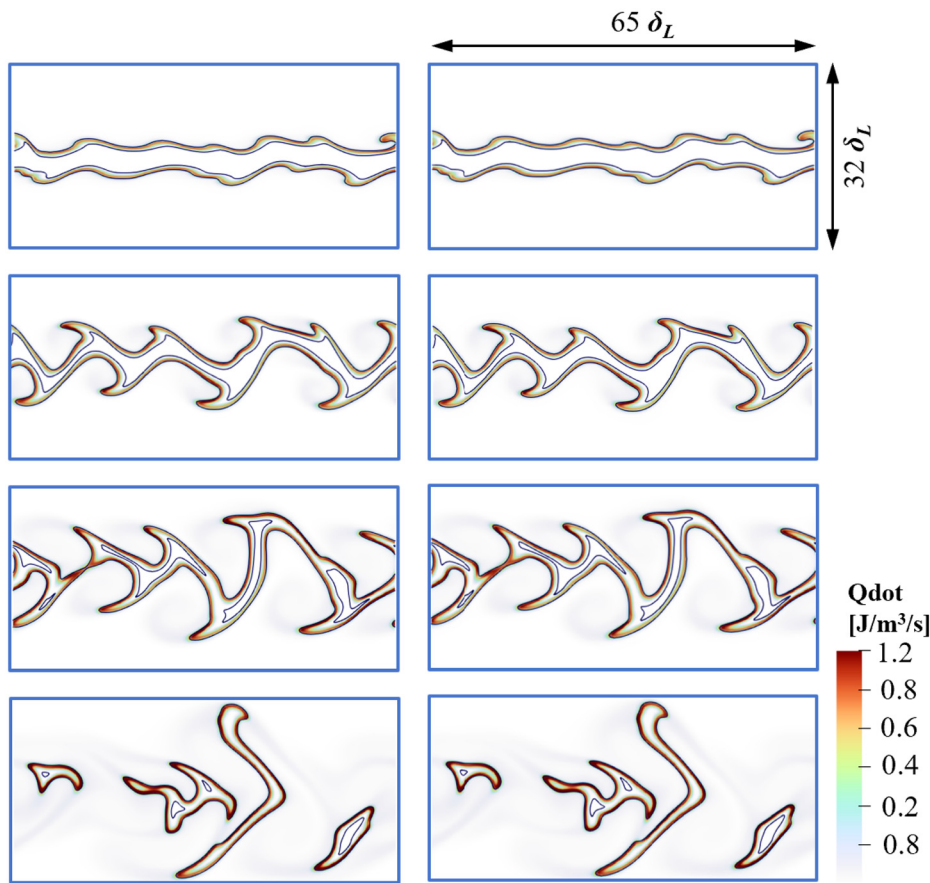
FIG. 9. Contours of heat release rate and isolines (black lines) for CH_2O with a mass fraction of 5×10^{-4} predicted using CVODE (left) and the DNN model (right) in the evolving jet flame of ethylene/air mixture at $t = 0.04$, 0.08, 0.12, and 0.16 ms.

species distributions predicted by the DNN align closely with the DI results, indicating high predictive accuracy even under turbulent conditions. Additionally, the turbulent burning velocity, S_T, is calculated using the following expression:

$$S_T = \frac{1}{A} \int_V \frac{\dot{\omega}_T}{c_p(T_b - T_u)} dV, \qquad (12)$$

where $\dot{\omega}_T$ is the heat release rate per unit mass, c_p is the specific heat capacity at constant pressure, T_b and T_u are the burnt and unburnt gas temperature, respectively, and A represents the equivalent flame front area. As seen in Fig. 10, the temporal evolution of S_T shows no observable discrepancy between the DNN model and DI predictions, further confirming the exceptional accuracy of the DNN model for turbulent flame simulations.
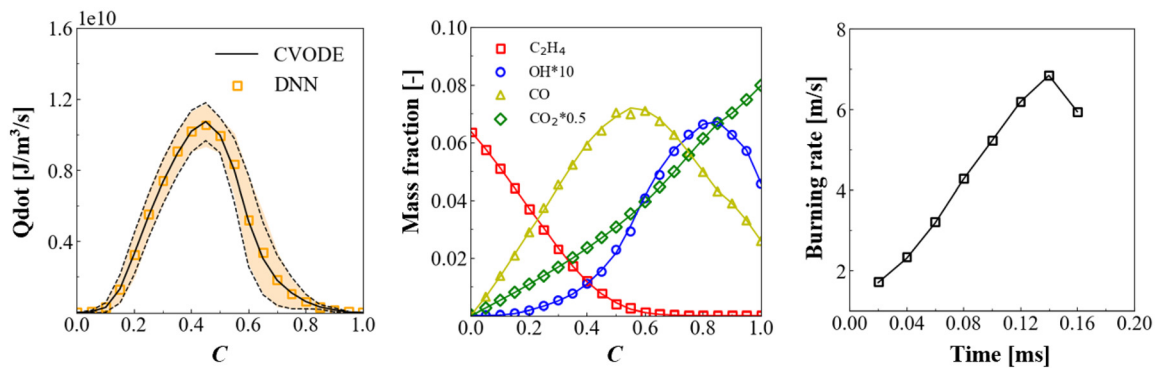

FIG. 10. Conditionally averaged Qdot (left, with standard deviation plotted) and mass fraction (middle) at $t = 0.12$ ms, and turbulent burning rate (right) in the evolving jet flame for ethylene/air mixture (lines from CVODE, symbols from DNN).

C. 2D HIT flame

The DNN model for ethylene/air combustion is further examined using the HIT propagating flame configuration. Figure 11 shows the contours of temperature distribution and flow vorticity over time in a stoichiometric mixture, providing a qualitative comparison of flame front structures affected by turbulence-chemistry interactions. As illustrated, the DNN model accurately captures flame front propagation and flame wrinkling behavior, showing close agreement with CVODE results.

For quantitative comparison, the turbulent burning velocity S_T is calculated using the formula above, where the flame front area A is approximated by the equivalent circumference of the burnt area. As shown in Fig. 12, the turbulent burning rates predicted by the DNN
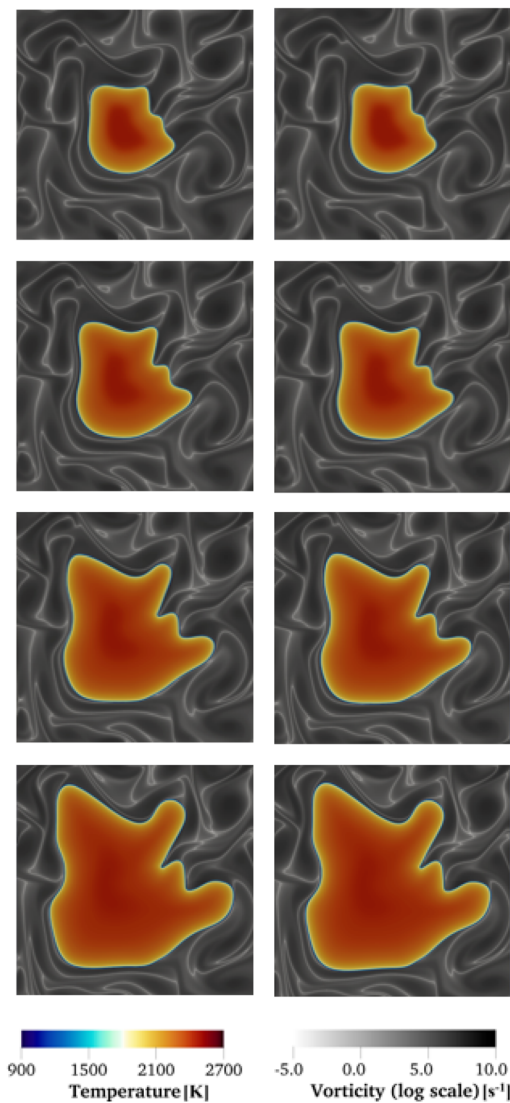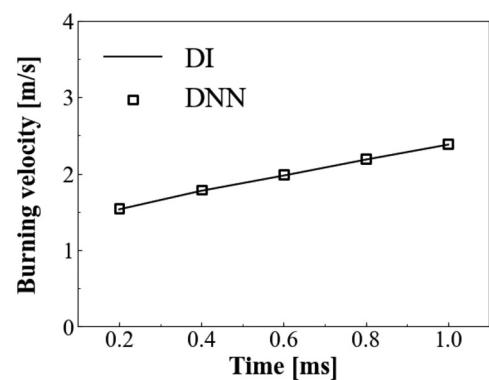

FIG. 12. Comparisons of instantaneous turbulent burning velocity in the propagating HIT flame of ethylene/air mixture.

model align well with those from CVODE, exhibiting a maximum prediction error of 0.72% for this complex chemistry. This level of accuracy indicates that the DNN model maintains reliable predictive capability even under the intense turbulence and chemical complexity of the HIT flame configuration.

D. Computational acceleration analysis

Following the above accuracy validations, the efficiency gain of the DNN approach is discussed. The overall computational time for a representative time period ($t = 0.3$–0.4 ms) in the propagating HIT flames is considered as an example. For the comparison shown here, the simulations with DI are run with 16 central processing units (CPUs) (AMD Zen1), while the simulations with DNN models use one GPU (NVIDIA RTX 4090) for inference. As seen in Table I, the DNN models achieve a speed-up factor of approximately 72 on chemistry calculations and 11 on overall calculations using one GPU for the ethylene/air case. Additionally, a higher speed-up factor of 102 on chemistry calculations and 13 for overall simulation is observed for the larger Jet-A/air mechanism. The proportion of computational time dedicated to chemistry is significantly reduced, from 87% to 13% for ethylene/air and to 11% for Jet-A/air when the DNNs are employed. This highlights a superior computational acceleration with the DNN models and suggests an increasing speed-up effect with the complexity of the chemical mechanism.

VI. CONCLUSIONS

This work performed consistent and comprehensive deep learning to develop DNN models across diverse fuels, with extensive

FIG. 11. Contours of time-evolving flame temperature and flow vorticity predicted using CVODE (left) and the DNN model (right) at $t = 0.4$, 0.6, 0.8, and 1.0 ms in the propagating HIT flame of ethylene/air mixture.

TABLE I. Computational time (hours) and speed-up factor of chemistry and total calculations for the 2D HIT flames.

	C$_2$H$_4$/air		JetA/air	
	Chemistry	Total	Chemistry	Total
CVODE	4.6	5.3	9.0	10.3
DNN	0.064	0.48	0.088	0.77
Speed-up	72×	11×	102×	13×

validations conducted to evaluate the models' precision and generalization capabilities in *a posteriori* flame configurations. The deep learning process involves collecting thermochemical base states from a small set of canonical laminar flames. To enhance the coverage of these base states in composition space for high-dimensional flames, an effective strategy involving random perturbation and data augmentation is employed, along with an essential constraint on heat release rate changes to eliminate nonphysical perturbed states. The resulting high-quality training samples serve as the input in the DNN training, wherein special considerations of data pre-processing and a four-hidden layer MLP balancing accuracy and efficiency are employed in the hyperparameter optimization process.

To evaluate the accuracy and computational efficiency of the trained DNN models in various reacting flow simulations, they are integrated into our recently developed open-source CFD package, DeepFlame, utilizing the high processing power of GPUs for model inference. Two representative turbulent reacting flow cases are established for *a posteriori* simulations. A comprehensive validation process is conducted, encompassing a range of laminar and turbulent flame configurations across different chemical systems, from simple hydrogen to complex jet fuel. The results obtained from the DNN models demonstrate excellent agreement with those from direct integration, highlighting the high accuracy and generalization capability of the employed deep learning approach as a versatile tool for integrating chemical reaction rates. Furthermore, computational acceleration using these DNN models yields promising speed-up factors of up to 100 for chemistry integration and approximately ten for the overall simulation. This observation suggests that stiff chemistry calculations will no longer be the computational bottleneck for turbulent flame simulations employing high-precision DNN models.

While the deep learning results presented in this work are encouraging, there remains room for improving the generalization ability toward large hydrocarbons and ammonia fuels with more multiscale chemical species involved. Notably, treating N_2 as an inert species is no longer valid for ammonia-based fuels, requiring a reevaluation of the randomization and normalization strategies, along with adjustments to the DNN model's output variables. Explicitly incorporating elemental conservation into the model's output could be a crucial step toward enhancing predictive accuracy. Future work will also be directed toward model compression and optimization to further enhance computational efficiency. Additionally, ongoing efforts are being dedicated to incorporating model inference into the solving procedure of partial differential equations (PDEs), aiming to achieve a full computation on the GPU. With the memory copy overhead eliminated, a further one or two orders of magnitude speed-up can be achieved.

SUPPLEMENTARY MATERIAL

See the supplementary material for DNN models and *a posteriori* CFD cases for model evaluation.

ACKNOWLEDGMENTS

AUTHOR DECLARATIONS
Conflict of Interest

The authors have no conflicts to disclose.

Author Contributions

Han Li and Ruixin Yang contributed equally to this work.

Han Li: Conceptualization (equal); Investigation (equal); Methodology (equal); Writing – original draft (equal). **Ruixin Yang:** Conceptualization (equal); Investigation (equal); Methodology (equal); Software (lead). **Yangchen Xu:** Validation (equal); Visualization (equal). **Min Zhang:** Methodology (supporting); Validation (supporting). **Runze Mao:** Software (supporting); Visualization (supporting). **Zhi X. Chen:** Conceptualization (equal); Resources (equal); Supervision (equal).

DATA AVAILABILITY

The data that support the findings of this study are available from the corresponding author upon reasonable request.

REFERENCES

[1] T. Poinsot and D. Veynante, *Theoretical and Numerical Combustion* (RT Edwards, Inc., 2005).

[2] S. Lam and D. Goussis, "The CSP method for simplifying kinetics," Int. J. Chem. Kinet. **26**, 461–486 (1994).

[3] T. Lu and C. Law, "A directed relation graph method for mechanism reduction," Proc. Combust. Inst. **30**, 1333–1341 (2005).

[4] P. Pepiot-Desjardins and H. Pitsch, "An efficient error-propagation-based reduction method for large chemical kinetic mechanisms," Combust. Flame **154**, 67–81 (2008).

[5] K. He, M. G. Ierapetritou, and I. P. Androulakis, "A graph-based approach to developing adaptive representations of complex reaction mechanisms," Combust. Flame **155**, 585–604 (2008).

[6] W. Sun, Z. Chen, X. Gou, and Y. Ju, "A path flux analysis method for the reduction of detailed chemical kinetic mechanisms," Combust. Flame **157**, 1298–1307 (2010).

[7] K. E. Niemeyer, C. J. Sung, and M. Raju, "Skeletal mechanism generation for surrogate fuels using directed relation graph with error propagation and sensitivity analysis," Combust. Flame **157**, 1760–1770 (2010).

[8] M. Ihme, W. T. Chung, and A. A. Mishra, "Combustion machine learning: Principles, progress and prospects," Prog. Energy Combust. Sci. **91**, 101010 (2022).

[9] F. Christo, A. Masri, E. Nebot, and T. Turányi, "Utilising artificial neural network and repro-modelling in turbulent combustion," in *Proceedings of ICNN'95-International Conference on Neural Networks* (IEEE, 1995), Vol. 2, pp. 911–916.

[10] J. Blasco, N. Fueyo, C. Dopazo, and J. Ballester, "Modelling the temporal evolution of a reduced combustion chemical system with an artificial neural network," Combust. Flame **113**, 38–52 (1998).

[11] J. A. Blasco, N. Fueyo, C. Dopazo, and J. Chen, "A self-organizing-map approach to chemistry representation in combustion applications," Combust. Theory Model. **4**, 61 (2000).

[12] B. A. Sen and S. Menon, "Turbulent premixed flame modeling using artificial neural networks based chemical kinetics," Proc. Combust. Inst. **32**, 1605–1611 (2009).

[13] B. A. Sen and S. Menon, "Linear eddy mixing based tabulation and artificial neural networks for large eddy simulations of turbulent flames," Combust. Flame **157**, 62–74 (2010).

[14] A. Chatzopoulos and S. Rigopoulos, "A chemistry tabulation approach via rate-controlled constrained equilibrium (RCCE) and artificial neural networks (ANNS), with application to turbulent non-premixed $CH_4/H_2/N_2$ flames," Proc. Combust. Inst. **34**, 1465–1473 (2013).

[15] L. L. Franke, A. K. Chatzopoulos, and S. Rigopoulos, "Tabulation of combustion chemistry via artificial neural networks (ANNS): Methodology and application to les-pdf simulation of Sydney flame l," Combust. Flame **185**, 245–260 (2017).

[16] K. Wan, C. Barnaud, L. Vervisch, and P. Domingo, "Chemistry reduction using machine learning trained from non-premixed micro-mixing modeling: Application to DNS of a syngas turbulent oxy-flame with side-wall effects," Combust. Flame **220**, 119–129 (2020).

[17] T. Ding, T. Readshaw, S. Rigopoulos, and W. Jones, "Machine learning tabulation of thermochemistry in turbulent combustion: An approach based on hybrid flamelet/random data and multiple multilayer perceptrons," Combust. Flame **231**, 111493 (2021).

[18] T. Readshaw, T. Ding, S. Rigopoulos, and W. Jones, "Modeling of turbulent flames with the large eddy simulation–probability density function (LES–PDF) approach, stochastic fields, and artificial neural networks," Phys. Fluids **33**, 035154 (2021).

[19] T. Zhang, Y. Yi, Y. Xu, Z. X. Chen, Y. Zhang, E. Weinan, and Z.-Q. J. Xu, "A multi-scale sampling method for accurate and robust deep neural network to predict combustion chemical kinetics," Combust. Flame **245**, 112319 (2022).

[20] M. P. Burke, M. Chaos, Y. Ju, F. L. Dryer, and S. J. Klippenstein, "Comprehensive h2/o2 kinetic model for high-pressure combustion," Int. J. Chem. Kinet. **44**, 444–474 (2012).

[21] K. Wu, W. Yao, and X. Fan, "Development and fidelity evaluation of a skeletal ethylene mechanism under scramjet-relevant conditions," Energy Fuels **31**, 14296–14305 (2017).

[22] R. Xu, K. Wang, S. Banerjee, J. Shao, T. Parise, Y. Zhu, S. Wang, A. Movaghar, D. J. Lee, R. Zhao *et al.*, "A physics-based approach to modeling real-fuel combustion chemistry–II. Reaction kinetic models of jet and rocket fuels," Combust. Flame **193**, 520–537 (2018).

[23] R. Mao, M. Lin, Y. Zhang, T. Zhang, Z.-Q. Xu, and Z. Chen, "Deepflame: A deep learning empowered open-source platform for reacting flow simulations," Comput. Phys. Commun. **291**, 108842 (2023).

[24] R. Mao, M. Zhang, Y. Wang, H. Li, J. Xu, X. Dong, Y. Zhang, and Z. X. Chen, "An integrated framework for accelerating reactive flow simulation using GPU and machine learning models," Proc. Combust. Inst. **40**, 105512 (2024).

[25] G. E. Box and D. R. Cox, "An analysis of transformations," J. R. Stat. Soc. Ser. B Methodol. **26**, 211–243 (1964).

[26] J. F. Driscoll, J. H. Chen, A. W. Skiba, C. D. Carter, E. R. Hawkes, and H. Wang, "Premixed flames subjected to extreme turbulence: Some questions and recent answers," Prog. Energy Combust. Sci. **76**, 100802 (2020).

[27] M. Saito, J. Xing, J. Nagao, and R. Kurose, "Data-driven simulation of ammonia combustion using neural ordinary differential equations (node)," Appl. Energy Combust. Sci. **16**, 100196 (2023).

[28] S. Karimkashi, H. Kahila, O. Kaario, M. Larmi, and V. Vuorinen, "A numerical study on combustion mode characterization for locally stratified dual-fuel mixtures," Combust. Flame **214**, 121–135 (2020).

[29] V. Vuorinen and K. Keskinen, "DNSLab: A gateway to turbulent flow simulation in Matlab," Comput. Phys. Commun. **203**, 278–289 (2016).

09 January 2025 09:22:57